ARCHIVIO ISTITUZIONALE
DELLA RICERCA

Alma Mater Studiorum Università di Bologna
Archivio istituzionale della ricerca

Early stages wind load assessment using Computational Fluid Dynamics: The new Bologna Stadium roof

This is the final peer-reviewed author's accepted manuscript (postprint) of the following publication:

Published Version:
Xing, J., Patruno, L., de Miranda, S., Pinardi, S., Majowiecki, M., Ubertini, F. (2023). Early stages wind load assessment using Computational Fluid Dynamics: The new Bologna Stadium roof. STRUCTURES, 47, 1912-1926 [10.1016/j.istruc.2022.11.089].

Availability:
This version is available at: https://hdl.handle.net/11585/956778 since: 2024-08-02

Published:

DOI: http://doi.org/10.1016/j.istruc.2022.11.089

Terms of use:

Some rights reserved. The terms and conditions for the reuse of this version of the manuscript are specified in the publishing policy. For all terms of use and more information see the publisher's website.

This item was downloaded from IRIS Università di Bologna (https://cris.unibo.it/).
When citing, please refer to the published version.

(Article begins on next page)

16 August 2024

Early stages wind load assessment using Computational Fluid Dynamics: the new Bologna Stadium roof

Jin Xing[a], Luca Patruno[a,], Stefano de Miranda[a], Stefano Pinardi[b], Massimo Majowiecki[b], Francesco Ubertini[a]

[a]*DICAM, University of Bologna, Viale del Risorgimento 2, 40136 Bologna, Italy*
[b]*Studio Tecnico Majowiecki, via Tizzano 46/2, 40033 Caralecchio di Reno, Bologna, Italy*

Abstract

The use of Computational Fluid Dynamics is rapidly expanding, allowing to complement traditional wind tunnel tests even in the case of extremely complex geometries at reasonable computational costs. In this contribution, we report the experience gained in the preliminary study of the new roof over the Bologna Stadium. The study, performed prior to wind tunnel tests, is meant to provide the designer a first evaluation of wind loads in early design stages, with classical wind tunnel tests planned at the final design stage. The most critical loading conditions are identified and the structural response evaluated. Finally, the structural response sensitivity to damping, which is difficult to be accurately evaluated *a priori*, is assessed. The study shows how early CFD simulations con effectively complement traditional wind tunnel tests in the project development.

Keywords: Wind loading, CFD, Large-span roofs, Large eddy simulation, Building Aerodynamics

List of acronyms

WTT	*Wind Tunnel Tests*
CFD	*Computational Fluid Dynamis*
LES	*Large Eddy Simulation*
ESWL	*Equivalent Static Wind Load*
PRFG^3	*Prescribed-wavevector Random Flow Generator 3-dimensional*
VBIC	*Variationally Based Inflow Correction*
POD	*Proper Orthogonal Decomposition*
PSM	*Proper Skin Mode*
ROM	*Reduced Order Model*

1. Introduction

As it is well-known wind-induced dynamic loading plays a crucial role in the design of large-span structures such as stadia [1, 2]. However, in modern architecture, the shape of the roof is characterized by high variability and providing general guidelines for the evaluation of wind loads acting on sub-horizontal surfaces is far from being an easy task. As a result, only a few standardized geometries are considered in codes and standards (see for instance [3, 4]), and extrapolating the case of interest starting from these known cases usually comes with great uncertainties.

For this reason, long-span roofs are usually tested by means of Wind Tunnel Tests, WTT, from which the time-varying pressure field acting on the roof is measured at several hundreds of points [5, 6]. Usually, based on the WT output, the structural dynamic response is numerically calculated [7, 8, 9]. With the structural responses for all wind attack angles, the extreme values of the response are calculated for each structural element, leading to the definition of the so called design envelope. Finally, Equivalent Static Wind Loads, ESWLs, might be calculated for design purposes [10, 11].

Although WTTs are well-established and widely adopted, their preparation is cumbersome and requires expensive infrastructures, so that great advantages might be obtained by using numerical simulations. In this context, the use of CFD is rapidly spreading, leading to the so called Computational Wind Engineering, CWE.

Nowadays CWE is routinely adopted in many applications such as pedestrian level wind

comfort and pollutant dispersion [12], but its use in the field of wind loads evaluation is still debated, at least from the point of view of codification. In particular, at the time of writing, the approach used by standards to regulate the use of CWE is extremely variable. The Japanese guidelines [13] provide a remarkable amount of details regarding the use of CWE, also proposing validation cases. On the contrary, Eurocode [3] and ASCE [14] substantially ignore CWE, but updates are expected to appear soon. Finally, the Italian guidelines [4] consider CWE in a dedicated informative annex. Despite such differences, which mainly arise due to some skepticism in using CWE for the final design, there is little doubt that CWE analyses can be extremely useful in the preliminary design stage, providing an intermediate step between the use of standard cases found on codes of practice and detailed WTTs.

Nevertheless, even in such context, the use of CWE for complex cases such as the analysis of a stadium roof is still uncommon. This is, at least partially, due to the fact that the use of computationally demanding scale resolving models is necessary for the assessment of structural vibrations [15, 16] and, thus, substantially mandatory even at the preliminary design stage for light structures.

In this paper, we present the preliminary study performed on the new roof of the Bologna Stadium, aimed at providing the designer a first evaluation of the structural response in the early stage of the design process, prior to the final design stage for which WTT are planned. The study makes use of Large Eddy Simulations, LES, as well as various techniques developed by the authors in recent years, which provide a smooth and comprehensive procedure for wind loading assessment. The combined use of such techniques proves essential in order to allow for an efficient and robust methodology without excessive overheads for the structural engineer, which is of great importance for preliminary analyses.

In particular, the structural response is calculated relying on the structural modes, but quasi-static corrections [17] are adopted in order to compensate for the truncation of the modal base. Such corrections are calculated relying on Proper Skin Modes, PSMs, which can be seen as a modal version of the standard approach based on influence coefficients, evaluated applying unitary forces [18].

As it will be seen, even for preliminary analyses, relatively high fidelity simulations are adopted and the structural response is calculated up to evaluating design values for each structural member. The analyses allow to make an early assessment, for instance, of locations showing particularly high peak pressures which can be used to guide the disposition of pressure taps in subsequent WTT, to individuate the most critical wind directions and study the effect of structural damping. In particular, such last aspect might be used in order to evaluate the opportunity to perform dedicated studies aimed at providing a more precise evaluation of such parameter and/or to guide the design of mitigation systems.

Finally, we also comment on the extraction of ESWLs which can be easily used for design purpose. In particular, ESWLs are here extracted by means of a slightly modified procedure with respect to that already presented by the authors [19] and they are used in order to provide to the designer static loads which can be used to refine predictions based on codes of practice.

We would like to stress that it is not the aim of this paper to provide an evaluation of LES models accuracy for large-roof structures, which would be impossible for the investigated case, as WTT have not been planned at the time of writing. What we aim to do here is to provide a description and assess the potential of numerical simulations as a complementary tool with respect to WTT, showing its practical application in a complex case.

The paper is organized as follows: in Section 2 the numerical settings of the LES analyses are outlined. The qualitative descriptions of the obtained flow fields are reported in Section 3. Subsequently, the calculation of the structural response and the extraction of ESWLs is discussed in Section 4. Finally, conclusions are drawn in Section 5.

2. Numerical model

In this section, the setup adopted for the CFD analyses is discussed. The geometry of the roof and the surroundings are described in Section 2.1, the adopted mesh and the numerical schemes are outlined in Section 2.2. Finally, in Section 2.3 the generation of turbulent inflow conditions is addressed.

2.1. Description of the Stadium

The stadium, Stadio Renato Dall'Ara, was built approximately a century ago and later deeply renovated for the 1990 FIFA World Cup. It currently has a capacity of more than 38000 people, as the home of the Bologna football club. The proposed project is to renovate the stadium and add a semi-closed large-span roof, designed by MJW structures [20]. The outline of the structure is depicted in Fig. 1 and its dimensions are planned to be 227 m in length and 160 m in width. The roof is located at a height of approximately 35 m and it is composed by an outer open-ring-like structure covered by opaque membranes and an inner translucent ring-like structure. The two are separated by a gap which allows the air flow and are supported by primary reticular structures (Fig. 1 (b)) and secondary curved beams (Fig. 1 (c)) surmounting them. The stadium roof is composed of approximately 4000 beams/trusses elements and it is subdivided into four sectors, shown in Fig. 1 (c). To be noticed is also the presence of a structure of height 42 m denoted Torre di Maradona, located at the middle of one of the long stadium sides.

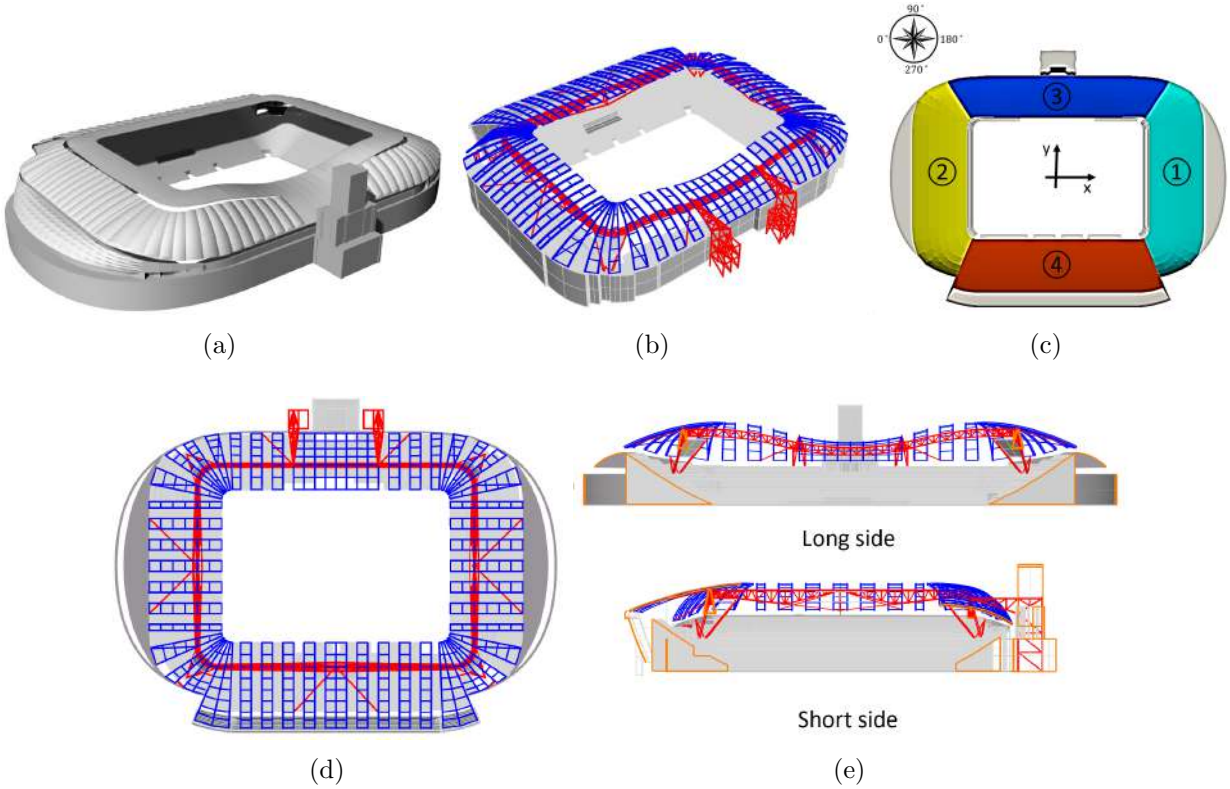

Fig. 1. The Bologna Stadium: (a) the view of the roof, (b) the primary (red) and secondary (blue) structures, (c) the roof subdivision into sectors, (d) plane view of the structural system and (e) vertical sections.

2.2. Numerical model for the wind flow simulation

We proceed at simulating the structure by means of Large Eddy Simulation, LES, in full-scale, but the Reynolds number is decreased by increasing the air viscosity of a factor 300 in order to increase the stability of the computations, i.e. by decreasing the cell Reynolds number [21]. This amounts to the fact that the simulated Reynolds number is comparable to that of a 1:300 scaled model, which is a quite standard scale for WTT. While numerical simulations are theoretically able to simulate full-scale conditions, this can hardly be obtained in practice if not for very simple cases or at high computational costs, which in this context appears unjustified due to the aforementioned consolidated WTT practice. The Reynolds number based on the roof height is approximately 2.94×10^5. The computational domain measures 1750 m, 1300 m and 340 m in length (streamwise direction), width and height, respectively, as shown in Fig. 2. The distance from the inlet to the stadium is 650 m.

The origin of the reference system is located on the ground at the center of the stadium. Neighboring buildings within a distance of 450 m are explicitly simulated. The first problem to be solved is that the stadium lies at the foot of the Apennines, so that the terrain varies remarkably in height within the area for which surroundings are explicitly reproduced. We decide to proceed with a rotor-stator approach as in standard WTT to avoid the need to re-mesh for each angle of attack (as all attack angles are obtained simply by rotating the rotor part). It is thus necessary, again in agreement with common WTT practice [4], to build a model in which the geometry of the hilly terrain is trimmed and smoothly connected to a flat surface representing the level imposed by the stator. The blockage ratio of the model is lower than 1%. All structural elements composing the roof have been removed (both main reticular beams, cables and secondary beams), so leaving only the main surfaces.

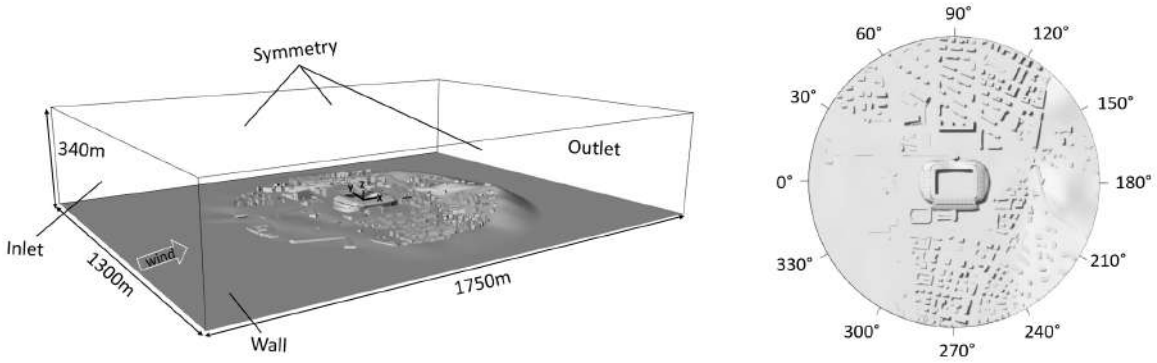

(a) (b)

Fig. 2. The computational domain: (a) overview and (b) the rotor with indication of wind attack angles.

The mesh size in the zone spanning from the inlet to the rotor has a maximum size of 6 m, in order to allow for the transport of the turbulence generated at the inflow up to the stadium without excessive dissipation. In the proximity of the stadium the mesh size is decreased up to approximately 1.5 m while in the proximity of the roof edges it is kept at approximately 0.75 m. The mesh is then coarsened downstream the rotor reaching a maximum size of 12 m. The total cell count is approximately 8.5 M.

The ground, the surroundings and the stadium surfaces are modeled as walls. The stadium roof is modelled considering the minimum thickness (0.2 m) which allowed to obtain

a good result in terms of meshing. Roughness has been added using rough wall-functions in the zones outside the rotor (where surroundings are not explicitly modelled) in other to match a Category III Eurocode terrain [3], while Van Driest damping is used for the stadium and the surroundings. Symmetry conditions are used on the top, front and the back surfaces of the domain, which are commonly used to model wind tunnel walls. The rotor and the stator are coupled by means of non-conforming interfaces, i.e. at the interface the mesh used for the rotor does not need to be the same as that used for the stator. The inlet boundary condition is generated using the synthetic turbulence generator, PRFG^3, discussed later in Sec. 2.3. A k-equation subgrid model is adopted [22].

Gradients and laplacians are calculated using the Gauss linear scheme while advective terms are approximated using the bounded linear scheme for k and the LUST scheme for the velocity field [23]. Pressure-velocity coupling is obtained with the well-known PISO algorithm [24] and time advancement is obtained using a Crank-Nicolson scheme blended with 10% backward Euler scheme. The pressure field is solved using the GAMG solver, while the velocity field is solved using the Gauss-Seidel smoother. Simulations are performed using OpenFoam 6.

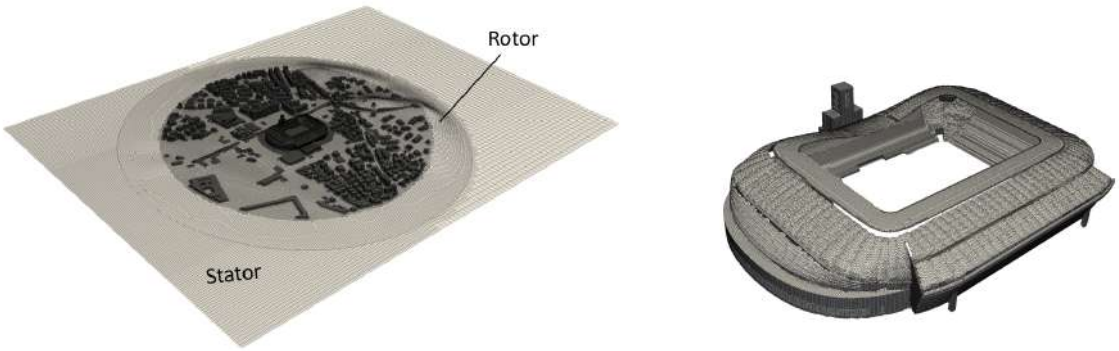

(a) (b)

Fig. 3. The adopted mesh: (a) overview and (b) details of the stadium (b).

To evaluate the wind effects on the stadium roof and predict the extreme wind loads, the simulation time should last for at least 700 s (600 s, i.e., 10 $mins$, for simulation and 100 s for model initialization). Notice that this is truly a minimum requirement as the

extraction of extreme values would require multiple samples of 10 *mins* each. However, this would strongly increase computational costs so that, for preliminary analyses, we here proceed considering only 1 sample of 10 *mins* for each angle of attack and consider a total of 12 wind attack angles, uniformly spaced every 30°, as indicated in Fig. 2 (b). The time step is 0.012 s, which leads to stable computations and to average Courant numbers around the stadium well-below 1 with extremes around 5 only in few small-size cells. To ensure the computational stability, the inflow velocity is ramped up from null value to the final value in 10 s. Each angle of attack is run on 192 *CPUs* and requires approximately 2800 *CPUh*.

The roof of the stadium is equipped with 3820 pressure taps, organized in 1910 pairs, i.e., on both upper and lower surfaces, to allow the measurement of net pressure, as indicated in Fig. 4 (a).

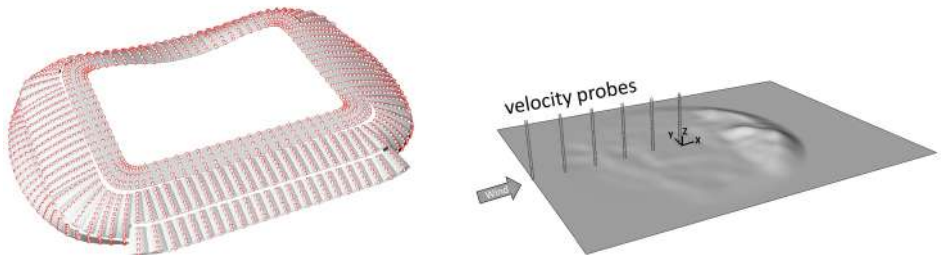

(a) (b)

Fig. 4. The distribution of the pressure probes on the stadium roof (a) and the velocity probes in the empty domain (b).

2.3. Synthetic turbulence inflow generation

According to the local wind climate, site roughness and code prescriptions, the inflow turbulence is generated based on the Category III Eurocode (EC) profile [3], assuming a base velocity of 25 m/s from all directions [4]. The reference height, H_r, is 40 m, so that the reference velocity there measured, U_r, is 27 m/s.

Firstly, a wind field in an empty domain is simulated to evaluate the wind profiles at the stadium location. Simulations have been run on both a completely empty domain and a domain in which the topography of the surroundings (without buildings) are considered, with the hilly part downstream the stadium to minimize its effect (Fig. 4 (b)). This is done

in order to make sure that the irregularity of the mesh close to the ground caused by the presence of the orographic elements does not cause excessive modifications of the profiles with respect to the completely empty case (which has a regular mesh close to the ground). The comparison between the two solutions, not here reported for the sake of brevity, did not highlight discrepancies between the two.

The turbulent inflow is generated through a turbulence synthesizer recently proposed by the authors, PRFG[3] and applied to the inflow patch using the VBIC technique, able to moderate pressure fluctuations induced by synthetic inflows. Readers are invited to refer to [25, 26, 27] for details. The comparison between the target and the simulated wind profiles are shown in Fig. 5. As can be observed, a good agreement can be obtained through the implemented turbulence synthetic generation procedure. The turbulence intensity of all three velocity components, u, v and w, at H_r is around 20%, 19% and 10%. Integral length scales reported in Fig. 5 (c) have been calculated using Taylor hypothesis of frozen turbulence from time-histories and are found in agreement with usual prescriptions. Notice that this is a parameter for which target values are known only very approximately, as large scatters are present in available site measurements.

As for the spectra at H_r, the results are presented in Fig. 6. The simulated results agree well with the targeted spectrum in the low-frequency region and show the classical cut-off frequency at approximately 0.6 Hz. In order to obtain such results, the turbulence intensity of all velocity components has been increased at the inflow of about 20% to compensate for the dissipation registered between the inflow and the stadium location. Avoiding such problem by refining the mesh, although surely preferable, would increase the computational cost substantially and, thus, such approach was not here followed. It shall be noticed that, aiming at calculating the structural response, the cut-off frequency shall be chosen in order to be higher than the structural vibration modes of interest, which in this case are in the order of $1Hz$ (see Sec. 4.1). Although not optimal, the present result is retained considering that the model in which the surroundings and the stadium are placed is characterized by mesh size 2 to 4 times finer than empty domain conditions, leading to a cut-off frequency

of 1.2 to 2.4Hz. Indeed, small scale structures will be produced by the explicitly simulated obstacles to a large extent, so that for preliminary simulations the obtained results appear to be acceptable.

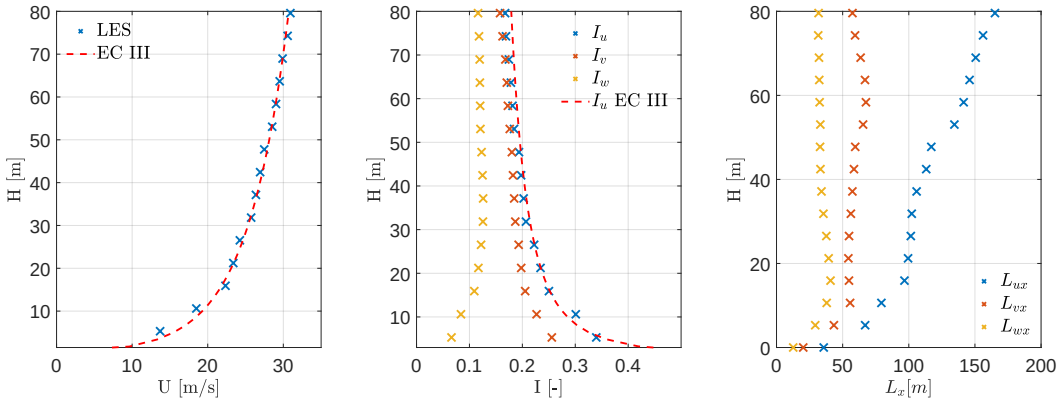

(a) (b) (c)

Fig. 5. Velocity profiles obtained from the empty domain test: (a) mean velocity profiles, (b) turbulence intensity profiles and (c) turbulence length scale profiles.

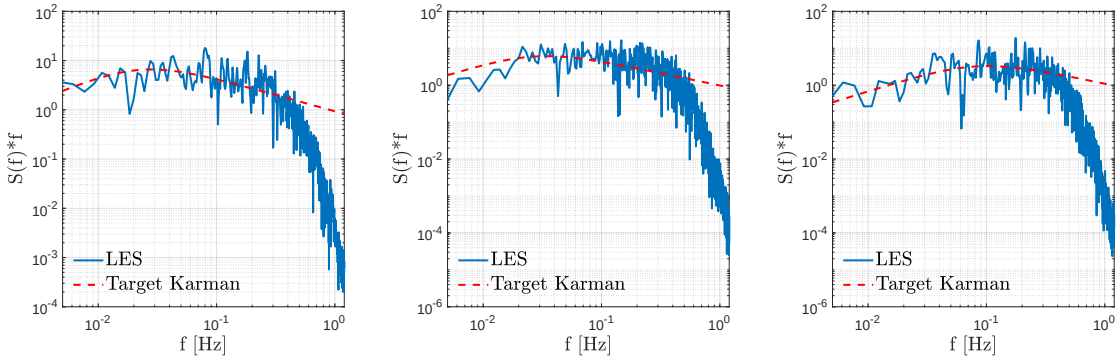

(a) (b) (c)

Fig. 6. Spectra of the velocity components measured at H_r: along-wind component (a), cross-wind component (b) and vertical component (c).

3. Characterization of the flow field

In this section, the simulated flow fields and the pressure distribution acting on the stadium roof are described. Firstly, in Section 3.1, the instantaneous flow fields obtained from the LES are presented. Then, the recorded pressure field is characterized in Section

3.2 and Section 3.3. Finally, global forces and moments are analyzed considering all wind attack angles.

3.1. Instantaneous flow field

Figure 7 reports the instantaneous flow fields represented by Q-criterion isosurfaces colored by U/U_r over the computational domain and the stadium, being U the instantaneous velocity magnitude. The turbulent structures produced by the stadium itself and the surrounding structures can be clearly seen, with the presence of large size vortices impinging on the roof oppositely to the side/corner they detach from.

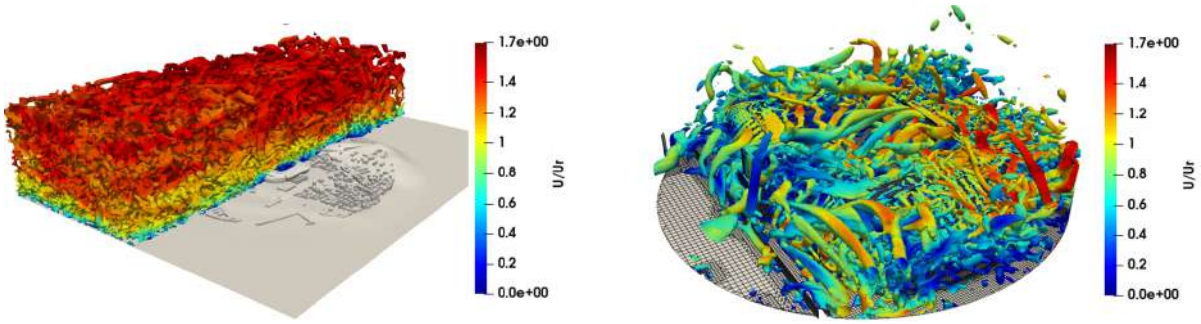

(a) (b)

Fig. 7. Overview of the flow field by means of instantaneous Q-criterion iso-surfaces colored by U/U_r: (a) overall domain ($Q = 0$) and (b) around the stadium at 120° ($Q = 2$).

Figure 8 shows two scenarios, with wind coming from the flat terrain part (30°) and the hilly terrain part (210°), respectively. In particular, the figure reports the value of the turbulent kinetic energy (not to be confused with the subgrid turbulent kinetic energy).

It can be seen that, as expected, while having a shielding effect on the stadium, the wind coming from the hill is expected to have stronger gusts compared to that coming from the flat terrain, so potentially leading to a larger dynamic response of the roof.

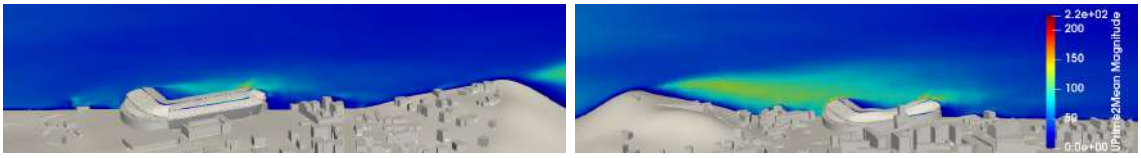

(a) (b)

Fig. 8. Flow visualization of the wind coming from different terrains, colored by $(|U'|/\bar{U})^2$: (a) 30° and (b) 210°.

3.2. Proper Orthogonal Decomposition

In order to characterize the pressure field acting on the stadium roof from different angles of attack, we here consider the well-known Proper Orthogonal Decomposition (POD). Readers interested in a methodological review of POD in wind pressure analysis can refer to [28]. In this context, we use POD decomposition mainly for two reasons. The first one is that it allows to obtain a synthetic characterization of the fluctuating pressure fields and make qualitative judgements relatively to the induced structural response. In fact, energy concentration in a few POD modes and their similarity to the structural modes shall be regarded as a situation prone to lead to large structural responses. Secondly, and even more importantly, numerical instabilities in the CFD models might lead to unexpected concentrated pressure fluctuations, easily identifiable observing the POD decomposition. In the best cases such instabilities lead to large fluctuations of the Courant number and, finally, to global instability of the simulation. Nevertheless, in some cases, they are more insidious and thus, a preliminary POD decomposition of the obtained results is always advisable.

Figure 9 shows the first POD mode of the pressure field when wind attack angles are 0°, 30°, 60°, 90°, 120° and 150°. As expected, for all considered wind attack angles, the highest pressure variations occur at the inner edge downstream the incoming wind direction. It can be seen that pressure fluctuations are concentrated on narrow stripes close to the edge for 90° angle of attack, so that it can be expected that such angles might be more relevant for the definition of local peak pressures than for the response of the primary structure. Contrarily, skew angles such as 60° lead to high levels of pressure fluctuations over all the longest span of the roof, so anticipating that they might be the more relevant incidence angle for the global

structural response evaluation.

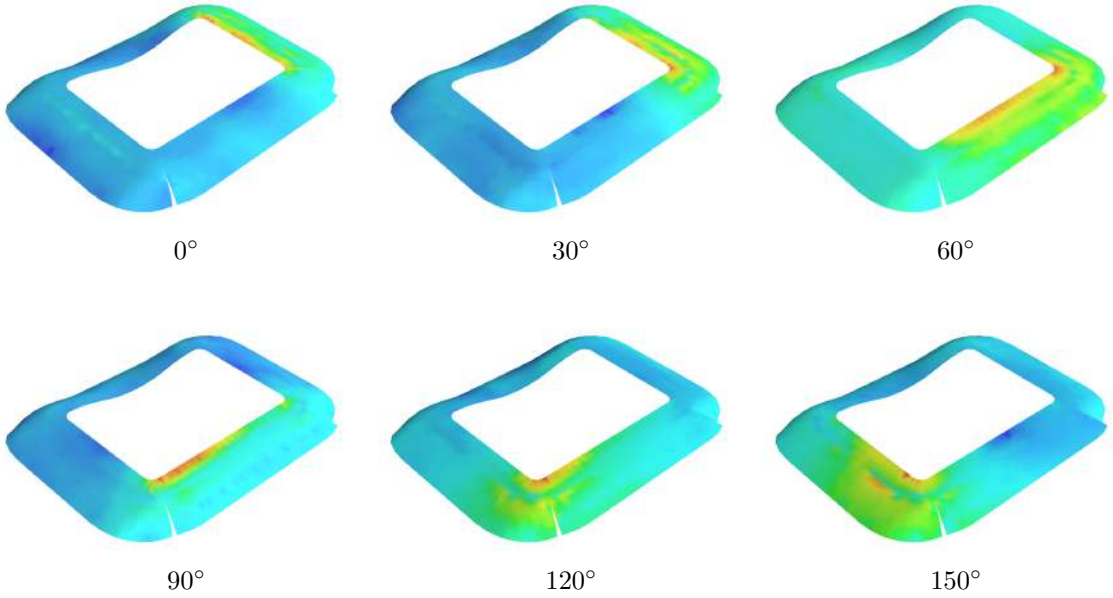

Fig. 9. Proper Orthogonal Decomposition, an overview of the first mode for angles up to 150° (colorbar not reported as the POD modes are not defined in amplitude).

For each case, the percentage of the total variance produced by the first POD mode is reported in Fig. 10 (a), while the number of POD modes necessary to cumulatively represent 25% and 75% of the total variance are shown in Fig. 10 (b) and (c).

Looking at Fig. 10 (a), we notice that the angles of attack showing the highest variance explained by only the first POD mode are those with the wind approaching from a short side (i.e., 0° and 180°). Conversely, those for which the explained variance is lower, correspond to the wind approaching orthogonal to the long side of the stadium. Looking now at Fig. 10 (b), in order to reach 25% of the total variance it is necessary to consider only 3 POD modes when the wind is approaching from a short side, while it takes up to 5 POD modes when the wind approaches from the long sides. Finally, considering Fig. 10 (c), we see that 40 to 50 POD modes are necessary to explain 75% of the total variance. Overall, data indicate that when the wind approaches orthogonal to the short sides, the aerodynamic excitation concentrates in a low number of modes and mainly affects the corresponding downstream sector. However, the excitation of the shorter sides is less demanding from the structural

point of view with respect to the long ones, so that the balance between such two aspects must be further analysed by calculating the structural response, as later reported.

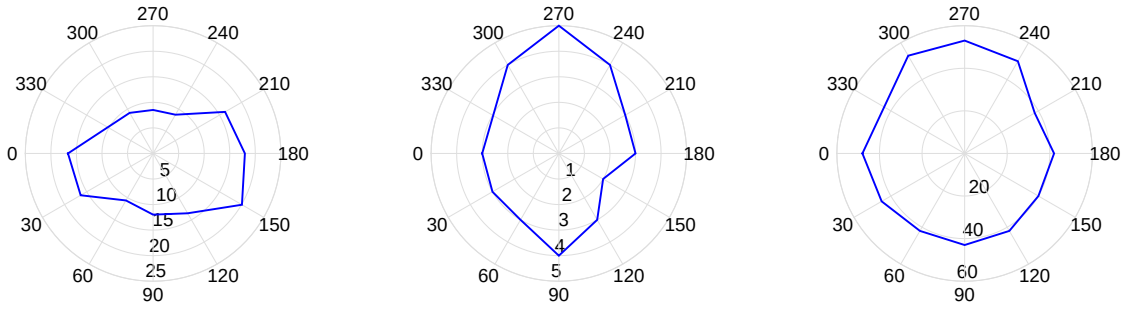

(a) (b) (c)

Fig. 10. Proper Orthogonal Decomposition of the pressure field: (a) energy of the first mode (percentage), (b) number of modes required to obtain 25% of total energy and (c) number of modes required to obtain 75% of total energy.

3.3. Peak pressure distribution

The peak pressure (i.e., minimum and maximum) distributions are presented in Fig. 11. Notice that we here always speak about the net pressure, difference between the top and bottom surfaces composing the roof. The extreme values are extracted for each monitor pair assuming a Gumbel distribution for the 10 *mins* peaks and calculating quantiles with non-exceedance probability equal to 80%, following the well-known Cook and Mayne approach [29]. It shall be noted that, as the duration of the simulated time series is 10 *mins*, it is necessary to extract quantiles related to 2 *mins* extremes and, then, shift them according to the well-known shifting property of the Gumbel distribution in order to recover the 10 *mins* peaks quantiles [30]. In essence, the approach assumes that the Gumbel distribution can fit the data with reasonable accuracy and that successive 2 *mins* extremes are independent. Notice that alternative solutions able to extract peak values from short time-histories have been recently proposed for instance in [31].

As expected, strong suctions and overpressures are predicted along the whole inner ring. The analyses suggest the presence of relatively high local pressures also in the proximity of the gap between the opaque and the translucent portions of the roof, which might be better

investigated in WTT.

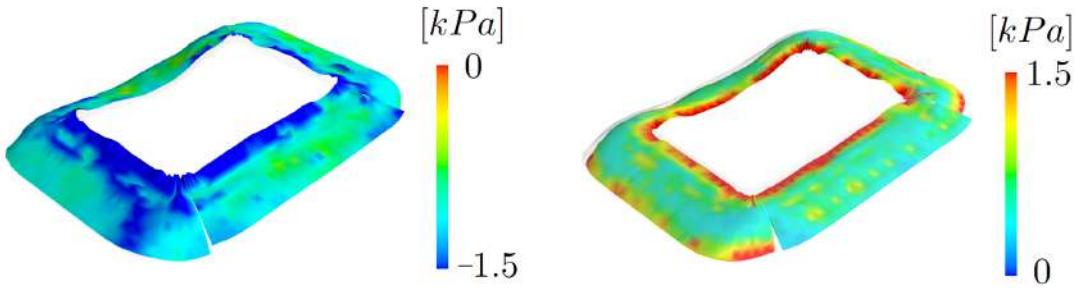

(a) (b)

Fig. 11. Peak pressures evaluated following Gumbel procedure with non-exceedance probability equal to 80% considering all attack angles: (a) minima and (b) maxima. The values are limited to the range -1.5 to 1.5 $[kPa]$ in order to allow an easier visualization of the distribution.

3.4. Global forces

Before proceeding to the evaluation of the structural response, we here consider the global forces acting on each roof sector (see Fig. 1 (c)). The time-averaged and the peak values of the global forces in the z direction, F_z, are show in Fig. 12. In particular, we report the time-averaged values, the gaussian envelopes (obtained by adding/subtracting to the mean 3 standard deviations) and the actually observed extreme values. Again, it can be clearly seen that for each sector the worst case condition is represented by the detachment of vortices from an upstream located sector. In some conditions (see for instance *Sector 4* at 60°), the response is strongly non-gaussian, so that the recorded extreme values fall outside the gaussian envelope. We notice that *Sector 3*, probably due to the particular curved shape which makes it stand at a lower height on average, does not appear to interact with vortices detached from *Sector 4*. Its response is generally gaussian with good approximation and more evenly distributed with the attack angle.

For the sake of completeness, we now provide a rough comparison between the obtained results and that which might be deduced applying codes and standards. In particular, the peak dynamic pressure coefficient, c_q can be evaluated as $c_q = 1 + 2gI_u$, being g a peak factor usually equal to 3.5. Considering that $I_u \approx 0.2$ at roof height according to the

present profile (see Fig. 5), $c_q = 2.4$. Comparing such value to the peak pressure coefficients reported in Fig. 12, suggests that: (a) the gaussain envelope, whose uplift maximum value is approximately 1.0 (*Sector 2*) suggests a pressure coefficient $c_p = 1.0/2.4 = 0.41$, (b) the actually measured maximum uplift value is 1.6 (still *Sector 2*) suggesting a pressure coefficient $c_p = 1.6/2.4 = 0.66$. Such values are well-comparable to those usually found for sub-horizontal structures in codes of practice (see for instance [4]), being a more precise comparison not possible due to the peculiarity of the considered shape.

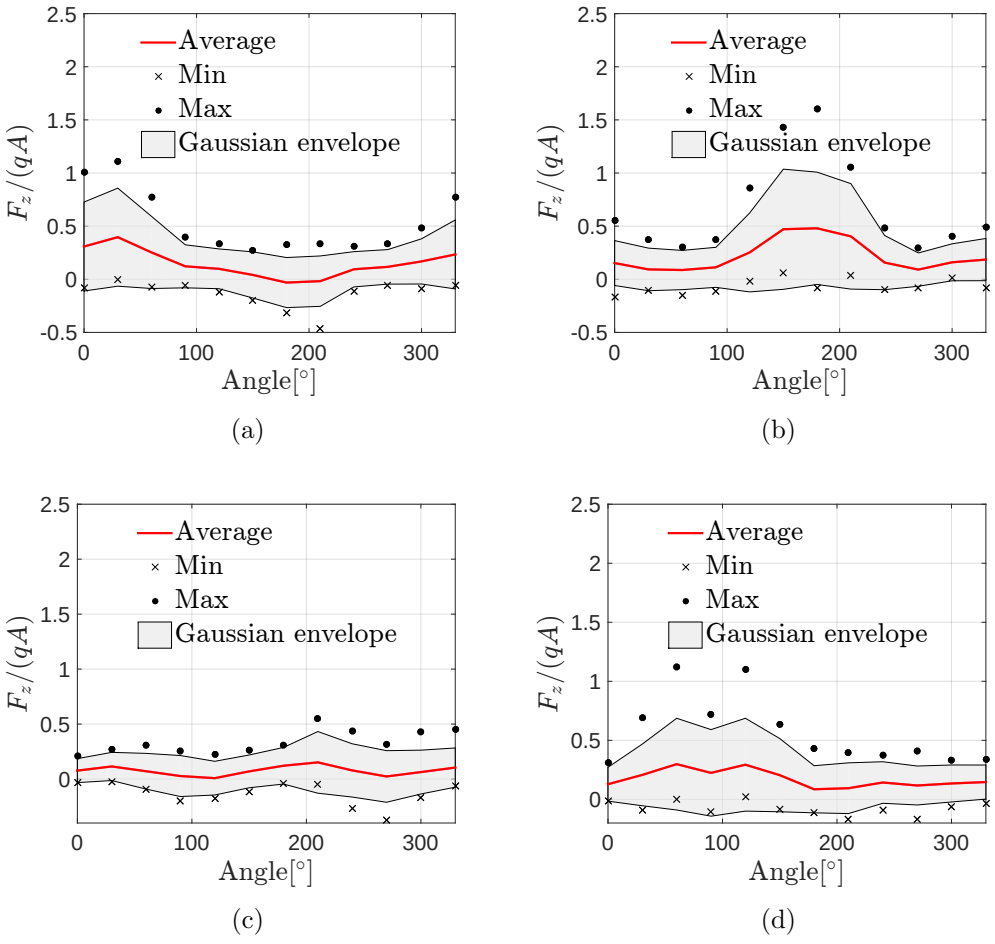

Fig. 12. Vertical force acting on each sector: (a) *Sector 1*, (b) *Sector 2*, (c) *Sector 3* and (d) *Sector 4*. Forces are made non-dimensional with respect to the reference pressure, $q = 0.5\rho {U_r}^2$, and the corresponding reference area, A.

Finally, Fig. 13 reports some meaningful statistics of the pressure filed at 60°, which can be seen from Fig. 12 to be one of the critical angles for *Sector 4*. The figures highlight

that very high values are observed at the roof edge, as expected, and that, due to the flow skewness, both $\bar{C}_p$, C'_p are slightly asymmetric, so also triggering an asymmetric structural response. Notice that extreme values reported in the figure are the extreme punctual unfiltered values measured during the analysis, so explaining the high recorded suction values.

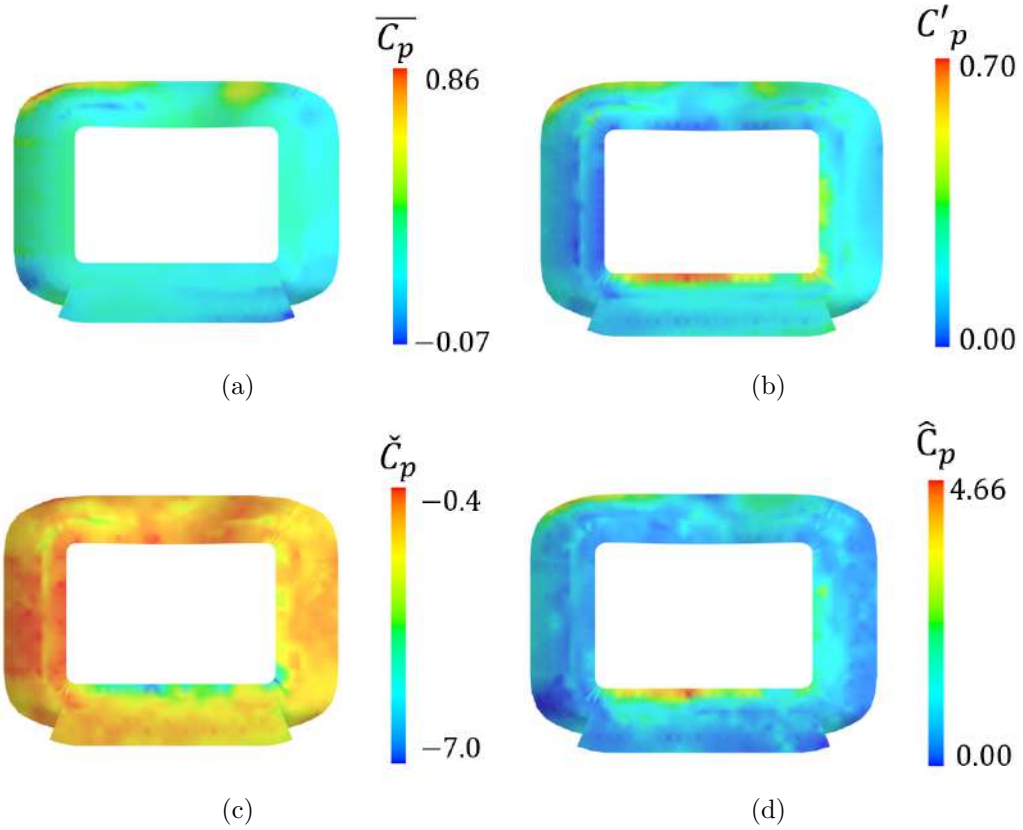

Fig. 13. The surface distributions of C_p statistics: (a) $\bar{C}_p$, (b) C'_p, (c) unfiltered recorded minima ($\check{C}_p$) and (d) unfiltered recorded maxima ($\hat{C}_p$).

4. Characterization of the structural response

In this section, we provide a description of the model used to evaluate the wind action over the roof. In particular, in Sec. 4.1, the mechanical behaviour of the structure is characterized by means of classical structural modes, complemented by the recently proposed Proper Skin Modes (PSMs). Then, in Sec. 4.2, we investigate the sensitivity of the results on the extreme value extraction method and the damping ratio (ξ). Finally, the extraction of ESWLs is discussed in Sec. 4.3.

4.1. Mechanical model

Characterizing the structural response with the purpose of assessing wind loading is relatively straightforward for simple idealized cases but it becomes often cumbersome in applications. The problem lies in the fact that the calculation of the structural response to wind excitation is usually performed by wind engineers outside the structural model software used by the designer. It is thus necessary to build a Reduced Order Model, ROM, of the structure in such a way that the required information can be easily extracted by general purpose commercial softwares, minimizing the overhead on the structural designer required to complete the task, e.g. the use of influence coefficients based on the application of punctual unit forces is theoretically simple but extremely impractical in practice. The procedure should be also conceived in order to be robust against gross human errors, which in the authors experience are extremely probable when reorganizing large datasets as required in this case.

In order to solve the problem, the authors devised a methodology based on the method of static corrections [18]. In particular, the ROM is built starting from usual structural modes, which are then complemented by Proper Skin Modes, PSMs. Such PSMs can be seen as a generalization of well-known influence coefficients based on the application of unitary forces, and actually, can be seen as their modal counterpart. We do not go into details here and interested readers are invited to refer to [18]. Nevertheless, the basic idea is that the structural response is calculated, as usual, in the modal base and static corrections are used to alleviate inaccuracies introduced by its truncation. Such static corrections are calculated by means of PSMs, which depend only on the surface geometry and can be easily calculated as the eigenvectors of a Laplacian operator discretized over the surfaces exposed to the wind action. This has also the positive effect to provide a robust way to check the model results: the response with and without static corrections shall be very similar.

An overview of the structural mode shapes is provided in Fig. 14 (only the ones relevant for wind loading are shown). It can be clearly seen that the mode shapes cannot be easily subdivided into global ones (affecting large parts of the structure and mainly the primary

structural system) and local ones (affecting small parts of the structure and mainly the secondary structural system). The situation if further complicated by the fact that the original structural model includes very massive parts as grandstands and surrounding walls, which tend to make the modes extraction difficult. Ideally, for the propose of studying the roof dynamics, it would be advisable to develop a model comprising only the roof and modelling the lower parts with restraints, fixing also all local vibration modes. This nevertheless adds remarkable overheads on the structural designer and decreases inter-operability. We thus decided to consider 100 modes, but even with such a large number, in this case it is difficult to asses the consequences of adopting a truncated modal base.

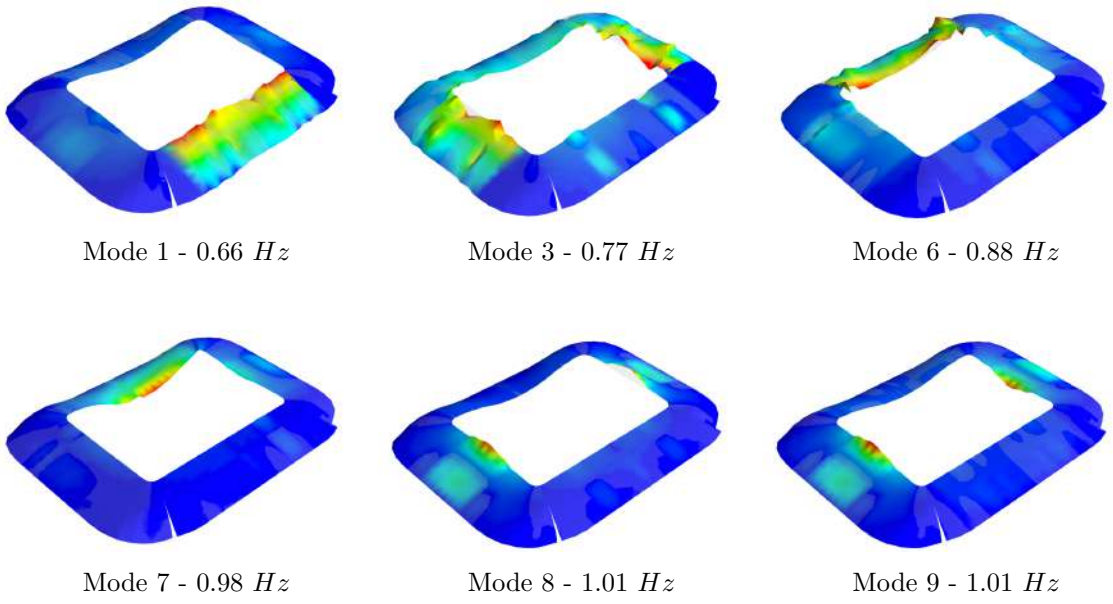

Fig. 14. Overview of the first ten structural modes, only those potentially relevant to wind loading are reported (colorbar not reported as the structural modes are not defined in amplitude).

We thus proceed at applying the approach proposed in [18], based on quasi-static corrections calculated from PSMs. In particular, the structural designer already subdivided the roof in four macro-areas. Five PSMs are extracted separately for each of them, as shown in Fig. 15. As it can be seen, the first PSM is always a constant, so taking into account for a uniform pressure distribution. Higher PSMs are naturally ordered by decreasing weavelength, so hierarchically subdividing the pressure field in components mainly affecting the

global response first, and the local response as the number of considered modes is increased. In this case, as we mainly investigate the global structural response, we consider only a few modes (5 for each roof sector, 20 in total) as the fifth PSM mode is the first one accounting for pressure variations from the outer to the inner ring (see Fig. 15 (c) and (f)). In practice, the procedure simply requires to transmit to the structural designer the 20 load distributions corresponding to the PSMs as nodal forces, run for each a static analysis and collect the results in terms of axial forces and bending moments and, eventually, displacements. The procedure is extremely efficient both in terms of computational time and work needed to extract the necessary information from the structural model, and can be applied to arbitrarily complex structures.

(a) PSM 1 (b) PSM 2 (c) PSM 5

(d) PSM 1 (e) PSM 2 (f) PSM 5

Fig. 15. Proper Skin Modes used in the structural response calculation: (a), (b) and (c) for the stadium curve and (d), (e) and (f) for the tribune.

Analyses made with and without static corrections, not here reported for the sake of conciseness, yield very similar results, so confirming that the model is correctly built and that the considered 100 modes allow for a good representation of the structural behaviour.

4.2. Sensitivity studies

Once the ROM for the structural response calculation is set up, it is possible to conduct structural analyses for each angle of attack and extract design envelopes (collecting for each member the design values of normal forces and bending moments).

Before proceeding, we deem important to assess the sensitivity of the model to two aspects/parameters which affect the analyses: the peak value extraction method and the adopted structural damping.

With respect to the first aspect, the same difficulties found for the local peak pressures arise here: the simulated time series are representative of 10 *mins* real scale, so that only one 10 *mins* return period extreme value can be extracted. Following the well-known Cook and Mayne approach [29], we target 80% quantiles. Those are estimated assuming a Gumbel distribution for the 2 *mins* extremes and extrapolating the 10 *mins* extremes by shifting it [30]. The approach is rigorously valid if the assumed Gumbel distribution is well-representative of the 2 *mins* extremes, but this is not necessarily the case. Also, by proceeding in this way, only 5 samples are available to estimate the distribution parameters, which potentially leaves space for statistical fluctuations. In order to have a simple check on the results obtained in this way, we firstly compare these results with the extremes actually observed in the time series. In particular, Fig. 16 and 17 show the scatter plot of the extreme values obtained with the two aforementioned methods, for axial forces and bending moments, respectively (for all structural members). In such figures, results directly observed in the time series are reported in abscissa (denoted as *MinMax*), while in ordinates the extreme obtained using Gumbel approach are shown. The correlation between the two results appears to be very good, with Gumbel approach providing on average slightly larger extremes, as expected (due to the fact that 80% non-exceedance probability was selected instead of 50%). This simple investigation cannot eliminate the opportunity to use longer time series to estimate quantiles (as usually done in WTT), but confirms that for early design stages, such aspect might be disregarded. From here on we thus proceed with the Gumbel approach.

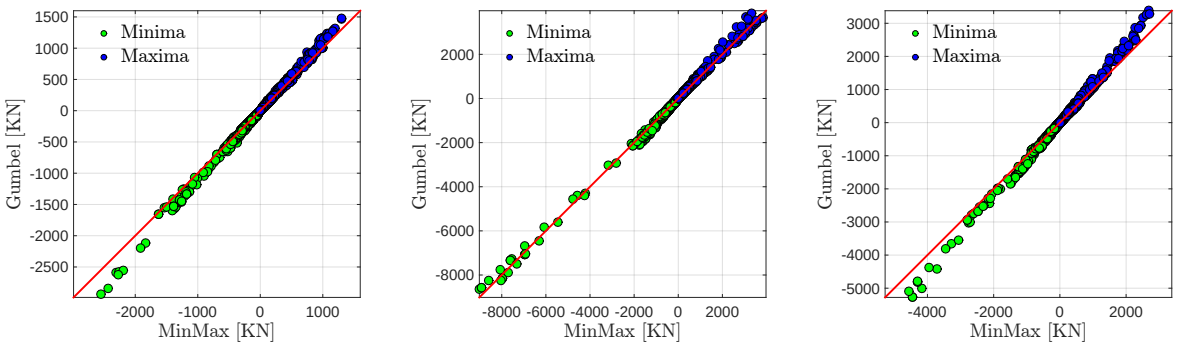

Fig. 16. Comparison between extreme values obtained using MinMax and Gumbel approach for axial forces: (a) 0°, (b) 60° and (c) 120°.

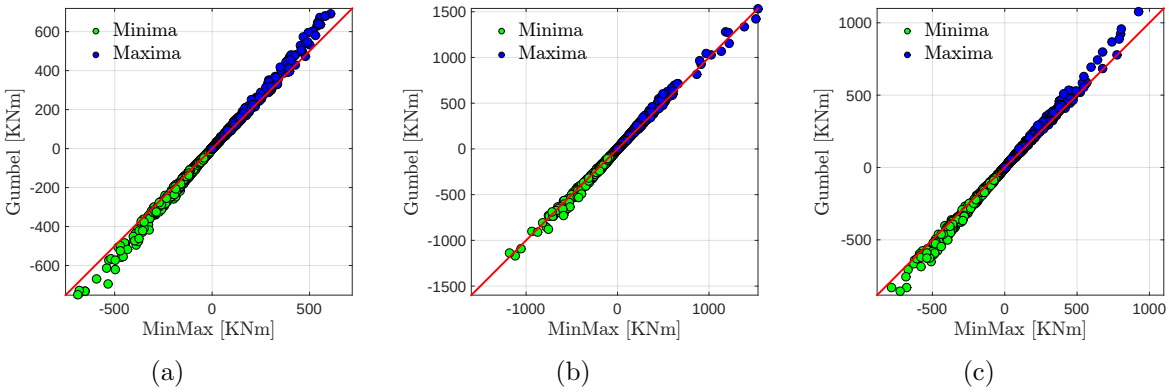

Fig. 17. Comparison between extreme values obtained using MinMax and Gumbel approach for bending moments: (a) 0°, (b) 60° and (c) 120°.

Once the extreme value extraction method is defined, it is necessary to carefully assess the effect of damping [32, 33], which is notoriously difficult to be evaluated *a priori*, also due to the presence of aerodynamic damping. Fig. 18 and 19 show the scatter plots between the design values (for each structural member) obtained with ξ, the damping ratio, equal to 0.01 and the corresponding values obtained with $\xi = 0.02$ and $\xi = 0.04$ (for all structural modes). The effect of ξ on the axial forces appears to be quite limited, while a deeper effect can be observed for bending moments. When ξ increases from 0.01 to 0.04, the peak axial forces decrease by about 37.5% for 60° and 25.0% for 120°, and the peak bending moments decrease about 50% for both cases. Such evaluations, although preliminary, can be used

in order to quantify the potential benefits obtainable from an explicitly dedicated in-depth study and/or the installation of appropriate damping devices. Aiming at obtaining results on the safe side, $\xi = 0.01$ is adopted in the following.

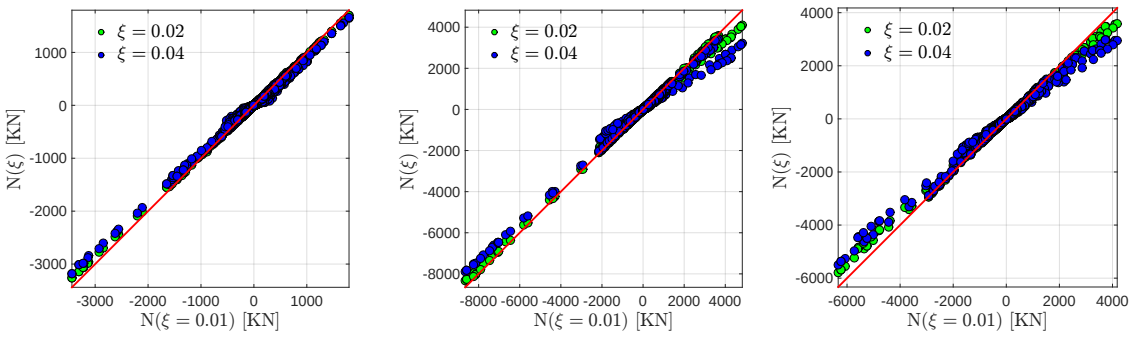

Fig. 18. Comparison between extreme axial forces obtained with different damping ratios: (a) 0°, (b) 60° and (c) 120°.

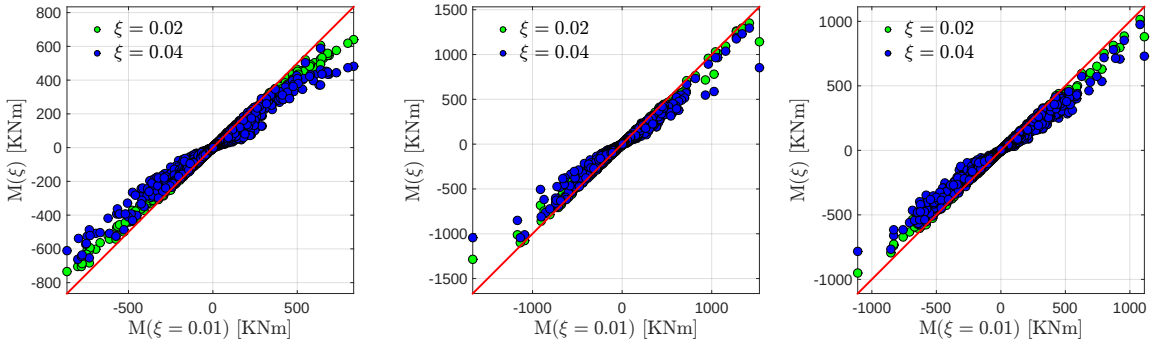

Fig. 19. Comparison between extreme bending moments obtained with different damping ratios: (a) 0°, (b) 60° and (c) 120°.

4.3. Design envelopes

We are now in the position to calculate the design values for each attack angle and, thus, the design envelopes. In this context it is useful to firstly consider the response obtained by making different hypotheses for the structural response calculation. In particular, Fig. 20 (axial forces) and Fig. 21 (bending moments) show the design envelopes obtained for different attack angles, considering the static (only time-averaged pressure field applied), the

quasi-static (dynamic amplification factor always equal to unity) and the dynamic structural response. The abscissa reports the structural element ID and the ordinate the calculated extreme values. Actually, for the sake of readability, only a part of the envelope is shown, with element ID ranging from 1950 to 2100, being the other parts of the envelope qualitatively similar. It can be seen that for many elements the static response is small, the quasi-static response counts for approximately half the dynamic response, being the other half provided by dynamic amplification. The quasi-static contribution can be substantially regarded as the limit case obtained for high damping levels, so that the potential benefits obtainable by refining the damping specification or installing damping devices can be evaluated for each structural element.

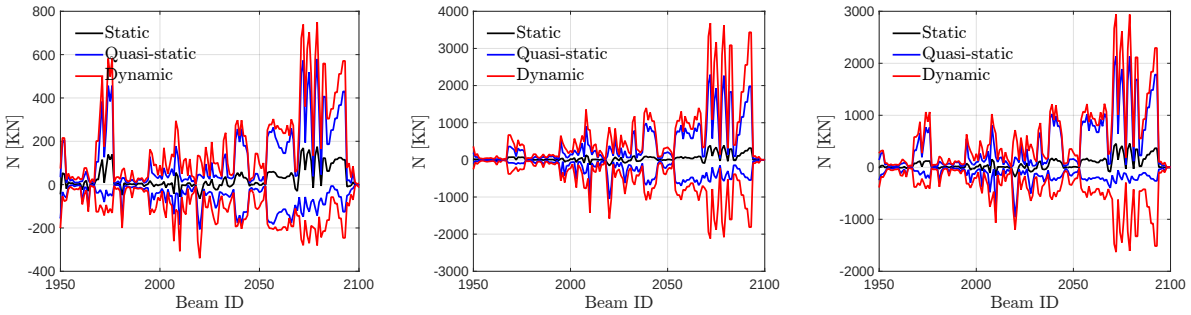

Fig. 20. Comparison between design envelopes for axial forces obtained from the static, quasi-static and dynamic components of the structure response: (a) 0°, (b) 60° and (c) 120°.

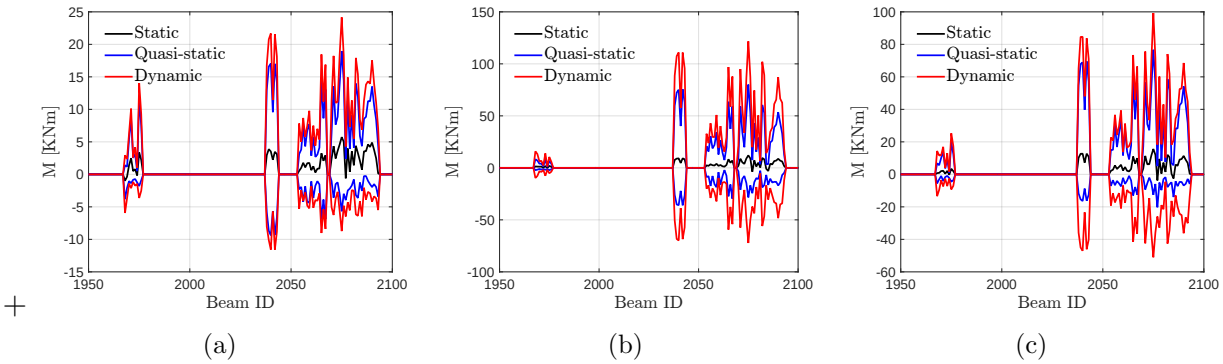

Fig. 21. Comparison between design envelopes for bending moments obtained from the static, quasi-static and dynamic components of the structure response: (a) 0°, (b) 60° and (c) 120°.

Finally, the envelope obtained by considering all attack angles with full dynamic analyses is reported in Fig. 22.

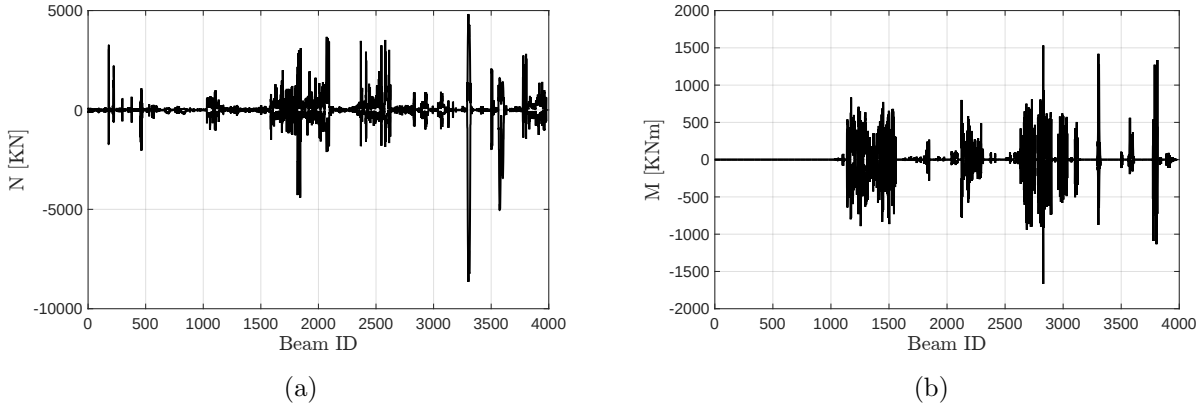

(a) (b)

Fig. 22. Design envelopes for all structural members considering all wind directions: (a) axial forces and (b) bending moments.

Figure 23 reports the percentage of elements which attain the extreme value (maximum and minimum) for each angle of attack. In other words, for each structural element, we individuate the wind angle of attack which yielded the design value. Notice that the two curves are similar, as expected, due to the fact that the response is oscillatory but they are not identical due to the time-average contribution and the dissymmetry (up-lifting and down-pushing) of the wind excitation. Clearly for both, axial forces and bending moments (Fig. 23 (a) and (b), respectively), there is a preferential direction along 60° and 240° which is responsible for the dimensioning of the majority of the structural elements, together contributing for approximately 40% of the design values. This again confirms that skew angles are the ones which lead to the most severe effects on the structure.

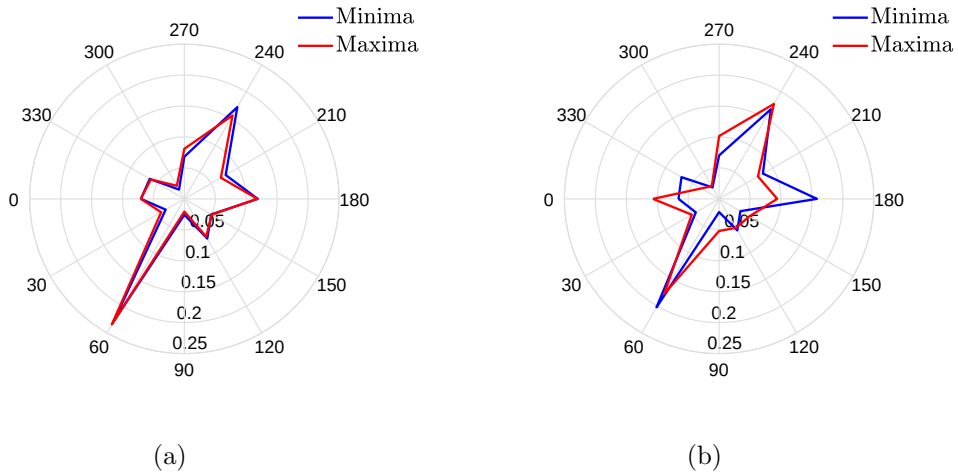

(a) (b)

Fig. 23. Percentage of structural elements attaining their design value of axial forces (a) and bending moments (b).

As a last step, we show the results obtained when converting the design envelopes in ESWLs. The procedure used to perform such passage are detailed in [19] and we here report in Appendix A only a very brief summary, useful to detail a slight modification here made to ameliorate the previously presented procedure.

Figure 24 reports the scatter plot between the design values calculated from dynamic analyses and those obtained from the application of ESWLs for axial forces. In particular, Fig. 24 (a), (b) and (c) show the results obtained using 3, 6 and 9 ESWLs respectively. Given the very good matching (results lying on the bisector) already obtained with 3 ESWLs, it means that the structural designer can safely design the main structure, which is composed mainly of truss elements, simply enveloping three static load conditions.

Unfortunately, in the case of the bending moments, which mainly compose the secondary structures, results appear less accurate, see Fig. 25. This is probably due to the more localized behaviour of the response, i.e. the secondary structures attain extreme values due to high/low pressure acting on smaller areas compared to the primary structural system. A higher number of PSMs might be considered to ameliorate results, if needed. In fact, we recall that PSMs are naturally ordered in such a way to firstly reconstruct the most uniform pressure distributions, mainly affecting the primary structural system, and then progressively

take into account local features of the pressure field, mainly relevant for secondary structural systems.

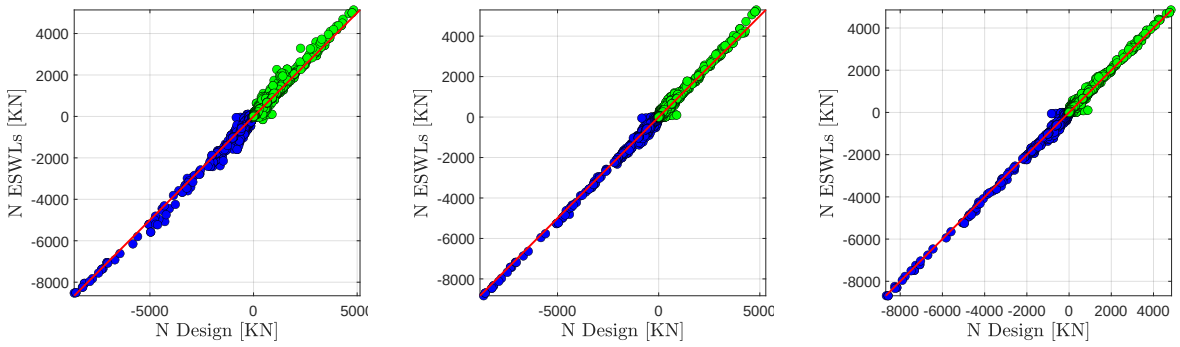

Fig. 24. Comparison between the design envelope for axial forces and values obtained from ESWLs: (a) 3 ESWLs, (b) 6 ESWLs and (c) 9 ESWLs.

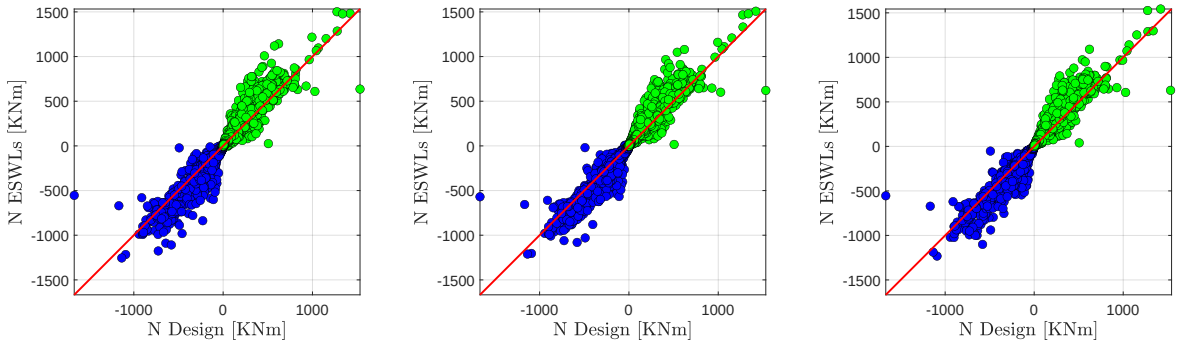

Fig. 25. Comparison between the design envelope for the bending moments and values obtained from ESWLs: (a) 3 ESWLs, (b) 6 ESWLs and (c) 9 ESWLs.

5. Conclusions

In this paper, we presented the preliminary analyses used to study the response of the new Bologna Stadium roof, taken as emblematic of a complex structure which might benefit from preliminary simulations to assess the effects induced by wind loading excitation. The analyses, run in the early stages of the design process and prior to WTT, have been used

to provide a first estimate of design values and, more importantly, to inform the subsequent steps of the design development.

In analogy to traditional experimental techniques, the study required the reconstruction of the stadium surroundings and the simulation of the wind flow has been obtained by means of LES. In order to obtain useful information for later design stages, the structural response has been calculated for all angles of attack and ESWLs extracted.

We individuate as key aspects which can benefit from an early assessment during the design process:

1. the expected effects/difficulties introduced by the presence of complex surroundings;
2. approximate individuation of regions characterized by high peak pressures;
3. the sensitivity to structural damping;
4. the evaluation of the relative importance of static, quasi-static and dynamic responses;
5. the individuation of wind directions which lead to stronger effects on the structures.

Thanks to such evaluations, it is possible to proceed to the final design with much deeper confidence regarding the absence of potentially unexpected behaviours and support decision regarding the most promising modifications and in-depth studies which might be undertaken to mitigate the wind-induced response.

Acknowledgments

The authors are thankful to CINECA for providing the HPC facilities which allowed the completion of the present study. The support provided by China Scholarship Council (CSC) is acknowledged.

Appendix A

The procedure used to perform such passage are detailed in [19] and we here report only a very brief summary, useful to detail a slight modification made to ameliorate the previously presented procedure. The interested reader is invited to refer to the original paper for details.

In short, ESWLs are built as combinations of PSMs which, once enveloped, reconstruct the design values. Taking as example the upper envelope, i.e. the maxima, the problem can be thus stated as

$$\boldsymbol{E}^{rec} = \max(\boldsymbol{E}^{psm}\boldsymbol{W}) = \max(\boldsymbol{E}^{eswl}) \approx \boldsymbol{E}^{env}, \tag{1}$$

where $\boldsymbol{E}^{env}$ is a vector which collects the extreme effects (e.g. axial forces and bending moments) for all the elements accounting for all attack angles obtained from dynamic analyses, $\boldsymbol{E}^{psm}$ are the effects induced by the PSMs, $\boldsymbol{W}$ is an unknown matrix of weighting coefficients to be determined and $\boldsymbol{E}^{rec}$ is the envelope reconstruction obtained from the ESWLs [34].

The identification of the matrix $\boldsymbol{W}$ which minimizes the difference between $\boldsymbol{E}^{env}$ and $\boldsymbol{E}^{rec}$ amounts to the determination of the ESWLs. It can be thus written that $\boldsymbol{W}$ is the matrix which minimizes the target function F_{max} with

$$F_{max} = ||\boldsymbol{E}^{env} - \boldsymbol{E}^{rec}||^2 = ||\boldsymbol{E}^{env} - \max(\boldsymbol{E}^{psm}\boldsymbol{W})||^2. \tag{2}$$

The details of such minimization are not here reported for the sake of conciseness and can be found in [19] and subsequent papers.

It is nevertheless important to realize that in the original procedure the upper and lower part of the envelope are reconstructed separately, so that one set of ESWLs is obtained to reproduce the maxima and another set is used to reproduce the minima. This is not optimal for design and might lead to over-conservative results. In fact, the procedure cannot ensure that, for instance, the ESWLs reconstructing the upper envelope do not exceed to lower one. To solve the problem, we here consider a modified target function, F, such that

$$F = ||\boldsymbol{E}^{envMax} - \max(\boldsymbol{E}^{psm}\boldsymbol{W})||^2 + ||\boldsymbol{E}^{envMin} - \min(\boldsymbol{E}^{psm}\boldsymbol{W})||^2, \tag{3}$$

where $\boldsymbol{E}^{envMax}$ is the upper design envelope (a vector collecting the maxima for each element) and $\boldsymbol{E}^{envMin}$ is the lower design envelope (a vector collecting the minima for each element). All the considerations reported in [19] for the minimization of Eq. (2) apply to Eq. (3). In fact, as F is the sum of two contributions, i.e. the first part related to the maxima

and the second one related to the minima, also the gradient of F is simply the sum of the corresponding two contribution, separately calculated.

The evaluation of the ESWLs can be also driven penalizing envelope underestimations more than overestimation, so that results are mainly on the safe side. It has also been highlighted that the present procedure shows strong affinities to Neural Network and in particular, to linear classification algorithms [35].

References

[1] M. Majowiecki, "Snow and wind experimental analysis in the design of long-span sub-horizontal structures," *Journal of Wind Engineering and Industrial Aerodynamics*, vol. 74, pp. 795–807, 1998.

[2] B. Vickery and M. Majowiecki, "Wind induced response of a cable supported stadium roof," *Journal of Wind Engineering and Industrial Aerodynamics*, vol. 42, no. 1-3, pp. 1447–1458, 1992.

[3] CEN, "Eurocode 1: Actions on structures, Part 1-4: General actions, Wind actions," *European Comitte for Standarization, Brussels, Belgium*, 2005.

[4] *CNR-DT R1 207/2018 Guide for the assessment of wind actions and effects on structures.* National Research Council Of Italy - Advisory Committee on Technical Recommendations for Construction; Rome, Italy.

[5] N. Su, S. Peng, and N. Hong, "Analyzing the background and resonant effects of wind-induced responses on large-span roofs," *Journal of Wind Engineering and Industrial Aerodynamics*, vol. 183, pp. 114–126, 2018.

[6] O. Nakamura, Y. Tamura, K. Miyashita, and M. Itoh, "A case study of wind pressure and wind-induced vibration of a large span open-type roof," *Journal of Wind Engineering and Industrial Aerodynamics*, vol. 52, pp. 237–248, 1994.

[7] M. Gu and X.-Y. Zhou, "An approximation method for resonant response with coupling modes of structures under wind action," *Journal of wind engineering and industrial aerodynamics*, vol. 97, no. 11-12, pp. 573–580, 2009.

[8] Y. L. Xu, W. Zhang, J. Ko, and J. Lin, "Pseudo-excitation method for vibration analysis of wind-excited structures," *Journal of Wind Engineering and Industrial Aerodynamics*, vol. 83, no. 1-3, pp. 443–454, 1999.

[9] D. Huang, L. Zhu, and W. Chen, "Covariance proper transformation-based pseudo excitation algorithm and simplified srss method for the response of high-rise building subject to wind-induced multi-excitation," *Engineering Structures*, vol. 100, pp. 425–441, 2015.

[10] M. Kasperski and H. Niemann, "The LRC (load-response-correlation)-method a general method of estimating unfavourable wind load distributions for linear and non-linear structural behaviour," *Journal of Wind Engineering and Industrial Aerodynamics*, vol. 43, no. 1-3, pp. 1753–1763, 1992.

[11] M. Gu and Y. Huang, "Equivalent static wind loads for stability design of large span roof structures," *Wind and Structures*, vol. 20, no. 1, pp. 95–115, 2015.

[12] B. Blocken, "50 years of computational wind engineering: Past, present and future," *Journal of Wind Engineering and Industrial Aerodynamics*, vol. 129, pp. 69–102, 2014.

[13] A. I. of Japan, "AIJ Guide for Numerical Prediction of Wind Loads on Buildings," *Tokyo, Japa*, 2005.

[14] ASCE, "Minimum Design Loads for Buildings and Other Structures," *American Society of Civil Engineers*, 2010.

[15] G. Lamberti and C. Gorlé, "Sensitivity of LES predictions of wind loading on a high-rise building to the inflow boundary condition," *Journal of Wind Engineering and Industrial Aerodynamics*, vol. 206, p. 104370, 2020.

[16] Y. Zhang, W. G. Habashi, and R. A. Khurram, "Predicting wind-induced vibrations of high-rise buildings using unsteady CFD and modal analysis," *Journal of Wind Engineering and Industrial Aerodynamics*, vol. 136, pp. 165–179, 2015.

[17] A. K. Chopra, "Dynamics of structures," 1975.

[18] L. Patruno, M. Ricci, S. de Miranda, and F. Ubertini, "An efficient approach to the evaluation of wind effects on structures based on recorded pressure fields," *Engineering Structures*, vol. 124, pp. 207–220, 2016.

[19] L. Patruno, M. Ricci, S. de Miranda, and F. Ubertini, "An efficient approach to the determination of equivalent static wind loads," *Journal of Fluids and Structures*, vol. 68, pp. 1–14, 2017.

[20] "MJW structures." https://www.majowiecki.com/. Accessed: 12-01-2022.

[21] C. Hirsch, *Numerical computation of internal and external flows: The fundamentals of computational fluid dynamics*. Elsevier, 2007.

[22] A. Yoshizawa, "Statistical theory for compressible turbulent shear flows, with the application to subgrid modeling," *The Physics of fluids*, vol. 29, no. 7, pp. 2152–2164, 1986.

[23] H. Weller, "Controlling the computational modes of the arbitrarily structured c grid," *Monthly Weather Review*, vol. 140, no. 10, pp. 3220–3234, 2012.

[24] R. Issa, "Solution of the implicitly discretised fluid flow equations by operator-splitting," *Journal of Computational Physics*, vol. 62, no. 1, pp. 40–65, 1986.

[25] L. Patruno and M. Ricci, "A systematic approach to the generation of synthetic turbulence using spectral methods," *Computer Methods in Applied Mechanics and Engineering*, vol. 340, pp. 881–904, 2018.

[26] M. Bervida, L. Patruno, S. Stanič, and S. de Miranda, "Synthetic generation of the atmospheric boundary layer for wind loading assessment using spectral methods," *Journal of Wind Engineering and Industrial Aerodynamics*, vol. 196, p. 104040, 2020.

[27] L. Patruno and S. de Miranda, "Unsteady inflow conditions: A variationally based solution to the insurgence of pressure fluctuations," *Computer Methods in Applied Mechanics and Engineering*, vol. 363, p. 112894, 2020.

[28] L. Carassale and M. Marré Brunenghi, "Statistical analysis of wind-induced pressure fields: A methodological perspective," *Journal of Wind Engineering and Industrial Aerodynamics*, vol. 99, no. 6, pp. 700–710, 2011. The Eleventh Italian National Conference on Wind Engineering, IN-VENTO-2010, Spoleto, Italy, June 30th - July 3rd 2010.

[29] N. Cook and J. Mayne, "A refined working approach to the assessment of wind loads for equivalent static design," *Journal of Wind Engineering and Industrial Aerodynamics*, vol. 6, no. 1, pp. 125–137, 1980.

[30] C. Dyrbye and S. O. Hansen, *Wind loads on structures*. 1997.

[31] M. Liu, X. Chen, and Q. Yang, "Estimation of peak factor of non-gaussian wind pressures by improved moment-based hermite model," *Journal of Engineering Mechanics*, vol. 143, no. 7, p. 06017006, 2017.

[32] J. Y. Kim, E. Yu, D. Y. Kim, and Y. Tamura, "Long-term monitoring of wind-induced responses of a large-span roof structure," *Journal of Wind Engineering and Industrial Aerodynamics*, vol. 99, no. 9, pp. 955–963, 2011. 9th UK Conference on Wind Engineering (September, 2010).

[33] M. Majowiecki and N. Cosentino, "Dynamic aspects of the new braga stadium large span roof," in *Proceedings of IASS symposium*, 2007.

[34] N. Blaise and V. Denoël, "Principal static wind loads," *Journal of Wind Engineering and Industrial Aerodynamics*, vol. 113, pp. 29–39, 2013.

[35] L. Patruno, M. Ricci, and S. de Miranda, "Buffeting analysis: a numerical study on the extraction of equivalent static wind loads," *Meccanica*, vol. 53, no. 4, pp. 671–680, 2018.